Analytical Theory of the Steady State Coastal Ocean and Equatorial Ocean

WOLFGANG FENNEL

Academy of Sciences of GDR, Institute of Marine Research, Rostock-Warnemünde, GDR

(Manuscript received 11 February 1987, in final form 27 November 1987)

ABSTRACT

Two linear stratified models—a coastal ocean on the f-plane and an unbounded equatorial β-plane—with Rayleigh friction and Newtonian cooling are examined. The problems are analytically tractable and a general formal solution can be formulated by means of a Green's function technique.

In particular the stationary response of a coastal ocean and an equatorial ocean to a longshore and a zonal wind patch, respectively, are calculated. Generally, the solutions are found as expansions of vertical modes.

The main purpose of this paper is to show that in certain cases the mode sums can be expressed by elementary functions. Thus closed analytical solutions are given for the coastal jet and the coastal undercurrent, as well as, the Yoshida jet and the equatorial undercurrent. Such expressions require various idealizations, in particular, a simple friction mechanism, constant or weakly varying Brunt–Väisälä frequency, a simple forcing structure, alongshore geostrophy in the coastal case, and the long-wave approximation in the equatorial case. In spite of these simplifications the solutions reproduce many of the observed features of the coastal and equatorial current systems.

The presented theory demonstrates the close relationships between some of the dynamical features of a coastal and an equatorial ocean mentioned earlier by Yoshida and Gill.

1. Introduction

As pointed out by Yoshida (1959) and later by Gill (1972) close relationships exist between some of the dynamical features of a coastal ocean and an equatorial ocean.

The response of a coastal ocean to a longshore wind patch consists of a downwind coastal jet confined to the upper mixed layer. Moreover, due to the propagation of coastal Kelvin waves excited at the edges of the wind patch an alongshore pressure gradient establishes which drives a coastal undercurrent. After a sufficiently long time the β-dispersion comes into play and then the jets decay into Rossby waves. This scenario has been described, e.g., by Philander and Yoon (1982).

Similarly, the response of an equatorial ocean to a zonal wind patch consists of a downwind jet, usually called Yoshida jet. Due to the excitation of eastward propagating Kelvin waves and westward propagating long Rossby waves at the edges of the wind band a zonal pressure gradient establishes which drives the equatorial undercurrent. This has been summarized by, e.g., McCreary (1981a), (1985). A further analytical study was presented by McPhaden (1981).

The resulting pattern is somewhat modified if the effects of meridional boundaries are taken into account, see McCreary (1981a). In particular, the surface jet will be reduced and the undercurrent will be somewhat enhanced.

The present paper is concerned with a further analytical study. Its main results consist in the derivation of closed analytical expressions for the coastal jet and the coastal undercurrent as well as for the Yoshida jet and the equatorial undercurrent.

The paper investigates the response to wind forcing of two linear stratified ocean models—a coastal ocean on a f-plane and an unbounded equatorial ocean. Dissipation is accounted for by Rayleigh friction and Newtonian cooling, the wind stress enters the ocean as a body force evenly distributed in the upper mixed layer. The underlying concept was outlined by, e.g., Gill (1982).

The model allows analytical solutions, which are given in terms of infinite sums over all vertical modes. In many cases the summations must be carried out numerically. Below we will discuss some examples where infinite series can be expressed by elementary functions.

The presented theory is close to McCreary (1981a,b). The main difference consists in the adopted friction mechanism. McCreary assumes the ocean to be diffusive where the vertical diffusivities of momentum and buoyancy are inversely proportional to N^2, where N is the Brunt–Väisälä frequency. This approach, which was firstly proposed by Fjeldstad (1963), is necessary to ensure separable solutions. This assumption has an important consequence; in the equations of motion of the individual vertical modes the resulting

Corresponding author address: Dr. Wolfgang Fennel, Akademie der Wissenschaften der DDR, Institut für Meereskunde, DDR 2530 Rostock-Warnemünde, Postschließfach 38, German Democratic Republic.

drag appears to be proportional to the square of the vertical eigenvalues. This implies that the higher vertical modes are much more affected by friction than the lower ones.

Contrary, Rayleigh friction and Newtonian cooling seems to affect all modes equally. It turns out, however, that due to the involved wave processes in the final solutions effective damping rates occur which are proportional to the vertical eigenvalues. Hence even in the frame of such a simple friction mechanism the higher vertical modes are stronger damped than the lower ones.

This paper is organized as follows: section 2 summarizes the governing equations and in section 3 the derivation of the formal solution is outlined. In section 4 the response of a stratified coastal ocean to a longshore wind band is studied and closed analytical expressions for the coastal jet and undercurrent are obtained. In section 5 we consider the response of an unbounded equatorial ocean to a stationary zonal wind patch. After some approximations of the involved infinite series of Hermite functions we find closed form solutions for the zonal velocity describing the Yoshida jet and the equatorial undercurrent. Finally, section 6 gives a summary and a discussion of the results.

2. Governing equations

We consider the linear Boussinesq equations with Rayleigh friction and Newtonian cooling, with the same relaxation constant r, in the form

$$\begin{aligned} u_t + ru - fv + p_x &= X \\ v_t + rv + fu + p_y &= Y \\ N^2 w + p_{zt} + rp_z &= 0 \\ u_x + v_y + w_z &= 0. \end{aligned} \tag{1}$$

The subscripts denote differentiation. The wind stress is assumed to enter the ocean as a body-force evenly distributed in the upper layer of thickness H_{mix}

$$(X, Y) \sim (u_*^2, v_*^2)\frac{\theta(z + H_{\text{mix}})}{H_{\text{mix}}} \tag{2}$$

where the friction velocities u_* and v_* are related to the wind stress components $\tau^{(x,y)}$ through

$$(u_*^2, v_*^2) = \frac{1}{\rho_0}(\tau^{(x)}, \tau^{(y)})$$

and $\theta(z + H_{\text{mix}})$ is the step function. Otherwise the notation is standard.

Assuming a flat bottom the solutions to (1) can be represented as expansions of vertical modes, $F_n(z)$, governed by the vertical eigenvalue problem

$$\begin{aligned} \left(\frac{d}{dz}\frac{1}{N^2}\frac{d}{dz} + \lambda_n^2\right)F_n(z) &= 0 \\ F_n'(0) = F_n'(-H) &= 0. \end{aligned} \tag{3}$$

Here the sea surface has assumed to be a rigid lid. This implies for the barotropic mode, $n = 0$, $F_0 = 1/\sqrt{H}$ and $\lambda_0 \to 0$. The solutions to (1) are then given by

$$\begin{aligned} (u, v, p, X, Y) &= \sum_{n=0}^{\infty}(u_n, v_n, p_n, X_n, Y_n)F_n(z) \\ w &= \sum_{n=1}^{\infty}\frac{w_n}{N^2}F_n'(z) \end{aligned} \tag{4}$$

where the expansion coefficients are functions only of x, y and t. For a constant Brunt–Väisälä frequency the normalized baroclinic eigenfunctions are

$$F_n(z) = \left(\frac{2}{H}\right)^{1/2}\cos\left(\frac{n\pi}{H}z\right) \tag{5}$$

with the corresponding eigenvalues

$$\lambda_n = \frac{n\pi}{NH} = n\lambda_1. \tag{6}$$

The projections of X and Y onto the F_n amounts to the expansion of the step function

$$\frac{\theta(z + H_{\text{mix}})}{H_{\text{mix}}} = \sum_{n=0}^{\infty}\frac{1}{h_n}F_n(z) \tag{7}$$

with

$$\frac{1}{h_0} = \frac{1}{\sqrt{H}}, \quad \frac{1}{h_n} = \left(\frac{2}{H}\right)^{1/2}\frac{\sin\left(\frac{n\pi}{H}H_{\text{mix}}\right)}{\frac{n\pi}{H}H_{\text{mix}}}. \tag{8}$$

Inserting the expansions (4) in (1) and Fourier transforming of the resulting equations with respect to x and t yields the following equations of the individual vertical modes

$$\begin{aligned} -i\bar{\omega}u_n - fv_n + ikp_n &= X_n \\ -i\bar{\omega}v_n + fu_n + p_{ny} &= Y_n \\ iku_n + v_{ny} - i\bar{\omega}\lambda_n^2 p_n &= 0 \\ w_n - i\bar{\omega}p_n &= 0 \end{aligned} \tag{9}$$

where $\bar{\omega} = \omega + ir$. For the coastal ocean model with a straight boundary at $y = 0$ the boundary conditions on the cross shore velocity v are

$$v = 0 \quad \text{at} \quad y = 0 \quad \text{and for} \quad y \to \infty. \tag{10}$$

In the case of an unbounded equatorial β-plane ocean the meridional velocity is subject to

$$v \to 0 \quad \text{for} \quad y \to \pm\infty. \tag{11}$$

If solutions to (9) and (10), or (11), are found, they must be inserted into (4) and then the final solutions follow after summation over all vertical modes.

Below we will see that for constant Brunt–Väisälä frequency certain mode sums can be performed explicitly. This, however, requires F_n, λ_n and h_n to de-

pend on the mode number n as in (5), (6) and (8), respectively.

Although we confine ourselves to the N = const case throughout this paper it seems worthy to note that those summations are possible also for weakly varying $N(z)$, where the WKB-treatment can be used. Assuming a constant N within the upper layer, $N = N_1$ for $0 \geqslant z \geqslant -H_{\text{mix}}$, the WKB-treatment yields

$$F_n(z) = \left(\frac{2N(z)}{H\bar{N}}\right)^{1/2} \cos\left(\lambda_n \int_z^0 N(z')dz'\right)$$

$$\bar{N} = \frac{1}{H}\int_{-H}^0 N(z)dz, \quad \lambda_n = \frac{n\pi}{\bar{N}H}$$

$$\frac{1}{h_n} = \left(\frac{2\bar{N}}{HN_1}\right)^{1/2} \frac{\sin\left(\pi n \frac{N_1}{\bar{N}} \frac{H_{\text{mix}}}{H}\right)}{\frac{n\pi H_{\text{mix}}}{H}}.$$

These quantities depend indeed on n as in the N = const case. Consequently all explicit summations of vertical mode series discussed below can also be performed with the aid of these WKB-expressions.

3. The formal solutions

In this section we summarize how the formal solutions to (9) with the boundary conditions (10) or (11) can be obtained. This can be accomplished by three steps. First, we derive an equation for v_n alone; second, we introduce the corresponding Green's functions, and then we express the solutions in terms of the Green's functions and the external forces, see Fennel (1986) and Fennel et al. (1987). The equation for v_n is

$$v_{nyy} + \alpha_n^2 v_n = \frac{i}{\bar{\omega}}(\bar{\omega}^2\lambda_n^2 - k^2)Y_n + \left(\lambda_n^2 f + \frac{k}{\bar{\omega}}\frac{d}{dy}\right)X_n. \tag{12}$$

In the case of a f-plane ocean α_n is given by

$$\alpha_n = (\lambda_n^2(\bar{\omega}^2 - f^2) - k^2)^{1/2}.$$

Next we introduce the corresponding Green's function $G(y, y')$ which is subject to

$$\left(\frac{d^2}{dy^2} + \alpha_n^2\right)G_n(y, y') = \delta(y - y')$$

$$G_n(0, y') = 0 \quad \text{and} \quad G_n(y, y') < \infty \quad \text{for} \quad y \to \infty.$$

The solution is

$$G_n(y, y') = \frac{1}{2i\alpha_n}(e^{i\alpha_n|y-y'|} - e^{i\alpha_n(y+y')}). \tag{13}$$

In the case of the equatorial β-plane the α_n^2 occurring in (12) is defined as

$$\alpha_n^2 = \bar{\omega}^2\lambda_n^2 - k^2 - \beta\frac{k}{\bar{\omega}} - \lambda_n^2 f^2, \quad f = \beta y$$

and the corresponding Green's function is governed by

$$\left[\frac{d^2}{dy^2} + \left(\bar{\omega}^2\lambda_n^2 - k^2 - \frac{\beta k}{\bar{\omega}} - \lambda_n^2\beta^2 y^2\right)\right]G_n(y, y') = \delta(y - y')$$

$$G_n(y, y') = 0 \quad \text{for} \quad y \to \pm\infty.$$

The solution is

$$G_n(y, y') = \sqrt{\lambda_n\beta}\sum_{m=0}^{\infty} \frac{\psi_m(\sqrt{\lambda_n\beta}y)\psi_m(\sqrt{\lambda_n\beta}y')}{\bar{\omega}^2\lambda_n^2 - k^2 - \frac{\beta k}{\bar{\omega}} - (2m+1)\lambda_n\beta} \tag{14}$$

where the ψ_m's are the normalized Hermite functions

$$\psi_m(\eta) = \frac{e^{-\eta^2/2}H_m(\eta)}{\pi^{1/4}\sqrt{2^m m!}}$$

with $H_m(\eta)$ being the Hermite polynomial of mth order.

If the Green's functions are known it is easy to express v_n by means of a source representation, and then the remaining observables can be expressed in terms of v_n. Thus we obtain

$$v_n(\omega, k, y) = \frac{i}{\bar{\omega}}(\bar{\omega}^2\lambda_n^2 - k^2)G_n * Y_n + \lambda_n^2 G_n * fX_n + \frac{k}{\bar{\omega}}G_n * X_{ny},$$

$$u_n(\omega, k, y) = -f\lambda_n^2 G_n * Y_n + \frac{k}{\bar{\omega}}G_{ny} * Y_n + \frac{i}{\bar{\omega}^2\lambda_n^2 - k^2}$$

$$\times\left[\lambda_n^2 X_n + \lambda_n^4 f G_n * fX_n + k\lambda_n^2 \times (fG_n * X_{ny'} - G_{ny} * fX_n) - \frac{k^2}{\bar{\omega}}G_{ny} * X_{ny'}\right]$$

$$p_n(\omega, k, y) = -\frac{fk}{\bar{\omega}}G_n * Y_n + G_{ny} * Y_n + \frac{i}{\bar{\omega}^2\lambda_n^2 - k^2}$$

$$\times\left[k(X_n + \lambda_n^2 f G_n * fX_n) - \bar{\omega}\lambda_n^2 G_{ny} * fX_n - kG_{ny} * X_{ny'} + \frac{k^2 f}{\bar{\omega}}G_n * X_{ny'}\right]. \tag{16}$$

The convolutions occurring in (16), e.g., $G_n fX_n$, are defined as

$$G_n * fX_n = f\int_0^{\infty} G_n(y, y')X_n(y')dy' \tag{17a}$$

in the f-plane case, and

$$G_n * fX_n = \int_{-\infty}^{+\infty} G_n(y, y')X_n(y')\beta y'dy' \tag{17b}$$

in the case of the equatorial β-plane. The other con-

volutions in (16) are defined by (17a, b) in an obvious manner.

From a theoretical standpoint the existence of such a general formal solution, which relates the dynamical fields to the external forcing, is very pleasing. The general structure of the solution is the same in both ocean models. Differences occur in the Green's functions and in the form of the convolutions. The only unknowns are the external forces which have to be modelled appropriately.

At this stage the formal solution applies to arbitrary $N(z)$ with the corresponding F_n and λ_n. Moreover, the damping mechanism used by McCreary (1981a,b) can be introduced simply by replacing r by $\lambda_n^2 A$, where A is related to some vertical diffusivities.

Generally, (16) describes the complete scenario of an oceanic response to any external wind. The analytical properties of the solution in the complex ω-plane correspond to the dynamical behavior of the responses. Thus in the case of the coastal ocean the Green's function (13) has branch points at $\bar{\omega} = (f^2 + k^2/\lambda_n^2)^{1/2}$, i.e., at those frequencies which define the dispersion relation of inertial waves.

In the case of the equatorial ocean the Green's function (14) has poles at frequencies determining the dispersion relation of equatorially trapped waves, e.g., see Moore and Philander (1977).

Moreover, in the equations of u_n and p_n in (16) we observe poles at $\bar{\omega} = k/\lambda_n$, which correspond to Kelvin waves, and some extraneous poles which, in particular, are associated with the "anti-Kelvin waves" $\bar{\omega} = -k/\lambda_n$. For an unbounded equatorial ocean these extraneous poles do not contribute to the final solutions as was shown by Fennel et al. (1987) in a general manner, where only the properties of the formal solution and of the Green's function have been used.

In the following sections we confine ourselves to the discussion of the steady state response to a wind patch given by

$$X(x, z) = \frac{-u_*^2}{H_{\text{mix}}}\,\theta(z + H_{\text{mix}})\theta(a - |x|), \quad Y = 0. \tag{18a}$$

Expansion of X into vertical modes and Fourier transforms with respect to x and t yields

$$X_n(\omega, k, y) = -\frac{u_*^2}{h_n}\,2\pi\delta(\omega)\,\frac{2\sin ka}{k}. \tag{18b}$$

In the case of a coastal ocean this describes an alongshore wind band, while for an equatorial ocean (18) models a zonal wind patch.

4. Response of a coastal ocean

In this section we consider the stationary response of a coastal ocean on a f-plane to a longshore wind patch as given by (18a,b). To this end we insert (18b) into the formal solution (16) and we use the Green's function (13) to estimate the involved convolutions according to (17a). The properties of the delta function imply $F(\omega)\delta(\omega) = F(0)\delta(\omega)$. Assuming, moreover, $r \ll f$ we have $\alpha_n^2(0, k) = -(1/R_n^2)(1 + k^2R_n^2)$ and it follows

$$u_n(\omega, k, y) = -\frac{u_*^2}{h_n}\,2\pi\delta(\omega)\,\frac{2\sin ka}{k}\,\frac{\lambda_n}{k^2 + r^2\lambda_n^2} \times\left[r\lambda_n\left(1 + \frac{G_n * 1}{R_n^2}\right) + \frac{ik}{R_n}\,G_{ny} * 1\right] \tag{19a}$$

$$v_n(\omega, k, y) = \frac{-u_*^2}{fh_n}\,2\pi\delta(\omega)\,\frac{2\sin ka}{k}\,\frac{G_n * 1}{R_n^2} \tag{19b}$$

$$p_n(\omega, k, y) = \frac{u_*^2}{h_n}\,2\pi\delta(\omega)\,\frac{2\sin ka}{k}\,\frac{1}{k^2 + r^2\lambda_n^2} \times\left[ik\left(1 + \frac{G_n * 1}{R_n^2}\right) + \frac{r\lambda_n}{R_n}\,G_{ny} * 1\right] \tag{19c}$$

where

$$G_n * 1\,|_{\omega=0} = \frac{R_n^2}{1 + k^2R_n^2}\,(e^{-(y/R_n)\sqrt{1 + k^2R_n^2}} - 1) \tag{20a}$$

$$G_{ny} * 1\,|_{\omega=0} = -\frac{R_n}{\sqrt{1 + k^2R_n^2}}\,e^{-(y/R_n)\sqrt{1 + k^2R_n^2}} \tag{20b}$$

and R_n is the Rossby radius, $R_n = (f\lambda_n)^{-1}$.

The inverse Fourier transforms with respect to k amount to certain convolutions involving the modified Bessel function K_0, e.g., Oberhettinger (1957). However, far enough from the corner points $y = 0$ and $x = \pm a$, i.e., for $y/R_1 \gg 1$ and $(x \pm a)/R_1 \gg 1$ the response is well approximated by the leading terms for small k. Then (20a, b) reduce to

$$G_n * 1 = R_n^2(e^{-y/R_n} - 1) \tag{21a}$$

$$G_{ny} * 1 = -R_n e^{-y/R_n}. \tag{21b}$$

Obviously, the assumptions $r \ll f$ and $(x \pm a)/R_1 \gg 1$ amount to assuming longshore geostrophy.

In the following two subsections we discuss the solution set (19), (21) in some detail starting with the case of an infinite longshore wind band, i.e., $a \to \infty$.

a. *Coastal jet*

For $a \to \infty$ we have $(2\sin ka)/k \to 2\pi\delta(k)$ and the solution is readily obtained

$$u_n(y) = -\frac{u_*^2}{h_n r}\,e^{-y/R_n} \tag{22a}$$

$$v_n(y) = -\frac{u_*^2}{h_n f}(e^{-y/R_n} - 1) \tag{22b}$$

$$p_n(y) = -\frac{u_*^2}{rh_n\lambda_n}\,e^{-y/R_n} \tag{22c}$$

$$w_n(y) = -rp_n(y). \tag{22d}$$

This describes the well-known coastal jet with the associated upwelling. The longshore current is geostrophically balanced by the cross-shore pressure gradient p_{ny}. In particular close to the coast the longshore flow is balanced by the wind, $ru_n(0) = -u_*^2/h_n$.

The final solution follows after summation over all vertical modes, according to (4). Introducing the sums

$$S_1(x, y, z) = H_{\text{mix}} \sum_{n=1}^{\infty} \frac{F_n(z)}{h_n} e^{-ny/R_1 - n\lambda_1 rx} \quad (23a)$$

$$S_2(x, y, z) = \frac{H_{\text{mix}}}{N} \sum_{n=1}^{\infty} \frac{F_n'(z)}{h_n \lambda_n} e^{-ny/R_1 - n\lambda_1 rx} \quad (23b)$$

from (4) and (22), we obtain

$$u(y, z) = -\frac{u_*^2}{rH_{\text{mix}}} [S_1(0, y, z) + H_{\text{mix}}/H] \quad (24a)$$

$$v(y, z) = -\frac{X}{f} - \frac{u_*^2}{fH_{\text{mix}}} [S_1(0, y, z) + H_{\text{mix}}/H] \quad (24b)$$

$$w(y, z) = \frac{u_*^2}{NH_{\text{mix}}} S_2(0, y, z). \quad (24c)$$

The sums S_1 and S_2 can be reduced to closed form expressions. With (5) and (8) we rewrite (23a, b) as

$$S_1(x, y, z) = \frac{1}{\pi} \sum_{n=1}^{\infty} (\sin n\varphi_+ + \sin n\varphi_-) \frac{e^{-n(y/R_1 + r\lambda_1 x)}}{n}$$

$$S_2(x, y, z) = \frac{1}{\pi} \sum_{n=1}^{\infty} (\cos n\varphi_+ - \cos n\varphi_-) \frac{e^{-n(y/R_1 + r\lambda_1 x)}}{n}$$

where

$$\varphi_\pm = \frac{\pi}{H} (H_{\text{mix}} \pm z).$$

Obviously S_1 and S_2 correspond to the imaginary and real part, respectively, of a sum of the type

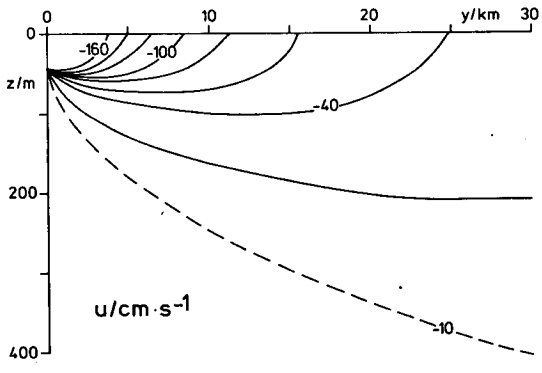

FIG. 1. Vertical section of the longshore current u showing the coastal jet. The contour interval is 20 cm s^{-1}. Isopleths higher than 160 cm s^{-1} are omitted. The maximum speed in the upper left corner is 242 cm s^{-1}.

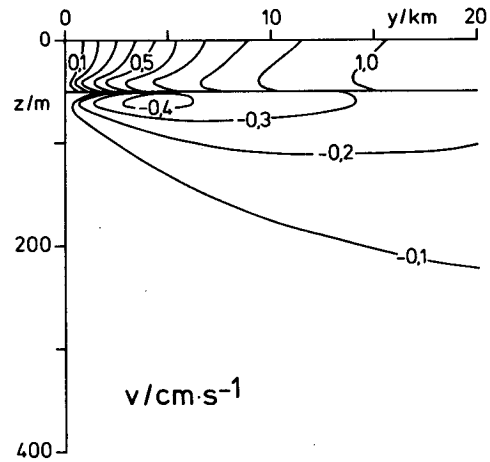

FIG. 2. Vertical section of the cross velocity v associated with the coastal jet. The contour interval is 0.1 cm s^{-1}.

$$\sum_{n=1}^{\infty} \frac{e^{-n(i\varphi+\gamma)}}{n} = -\ln(1 - e^{-(i\varphi+\gamma)})$$

$$= -\ln(|1 - e^{-(i\varphi+\gamma)}|) - i \arg(1 - e^{-(i\varphi+\gamma)}).$$

This implies

$$S_1(x, y, z) = \frac{1}{\pi} \left[\arctan\left(\frac{\sin\varphi_+}{e^{y/R_1 + r\lambda_1 x} - \cos\varphi_+} \right) + \arctan\left(\frac{\sin\varphi_-}{e^{y/R_1 + r\lambda_1 x} - \cos\varphi_-} \right) \right] \quad (25a)$$

$$S_2(x, y, z) = \frac{1}{2\pi} \ln\left[\frac{\cosh(y/R_1 + r\lambda_1 x) - \cos\varphi_-}{\cosh(y/R_1 + r\lambda_1 x) - \cos\varphi_+} \right]. \quad (25b)$$

Putting in (25) $x = 0$, we have the mode sums occurring in (24) expressed by elementary functions.

We note that the pressure is proportional to a sum of the type

$$\sum_{n=1}^{\infty} \frac{e^{-n(i\varphi+\gamma)}}{n^2}. \quad (26)$$

For $\gamma = 0$ this sum can only be expressed in terms of elementary functions. For nonzero γ (26) is related to the Dilogarithm which is a nonelementary transcendental function, e.g., Abramovitz and Stegun (1984).

In Figs. 1, 2 and 3 sketches of u, v and w are displayed, where the involved parameters are chosen as $H = 1000$ m, $H_{\text{mix}} = 50$ m, $u_*^2 = 0.5$ cm^2 s^{-2}, $f = 7.5$ 10^{-5} s^{-1}, $r^{-1} = 30$ days, and $R_1 = 40$ km. In particular, Fig. 1 shows the coastal jet which is surface trapped and whose maximum speed at the coast, $y = 0$, is set by u_*^2/rH_{mix}. Due to the highly idealized geometry of the model the vertical velocity has a logarithmic singularity at the point $y = 0$, $z = -H_{\text{mix}}$, compare (24c) and (25b). Such a singularity does not occur in the

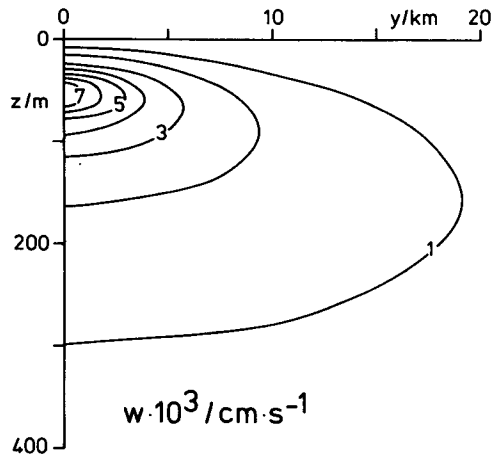

FIG. 3. Vertical section of the vertical velocity w associated with the coastal jet. The contour interval is 10^{-3} cm s^{-1}. The vertical velocity is multiplied by 10^3. At the point $y = 0$ and $z = -H_{\text{mix}}$ there occurs a weak logarithmic singularity.

coastal jet solution of McCreary (1981b). This indicates that using heat diffusion rather than Newtonian cooling removes the singularity. However, the horizontal speed is too high in McCreary's model.

The dynamical balances of the coastal jet regime are

$$ru - fv = X, \quad \text{with} \quad ru = X \text{ at the coast,}$$

$$\text{and} \quad -fv = X \quad \text{for} \quad y \to \infty$$

$$fu + p_y = 0,$$

$$v_y + w_z = 0. \tag{27}$$

The flow is two-dimensional and the offshore Ekman current is balanced by the coastal upwelling.

b. Coastal undercurrent

Next we wish to analyze the response to a wind patch (compare Fig. 4) according to (19) and (21). The solutions are

$$u_n(x, y) = \frac{-u_*^2}{rh_n} e^{-y/R_n}[\theta(a - |x|) - \theta(x + a)e^{-(x+a)\lambda_n r} + \theta(x - a)e^{-(x-a)\lambda_n r}] \tag{28a}$$

$$v_n(x, y) = \frac{u_*^2}{fh_n} \theta(a - |x|)(1 - e^{-y/R_n}) \tag{28b}$$

$$p_n(x, y) = \frac{-u_*^2 e^{-y/R_n}}{rh_n\lambda_n} [\theta(a - |x|) - \theta(x + a)e^{-(x+a)\lambda_n r} + \theta(x - a)e^{-(x-a)\lambda_n r}] \tag{28c}$$

$$w_n(x, y) = -rp_n(x, y). \tag{28d}$$

Because of the rigid-lid condition, implying $\lambda_0 \to 0$ and $R_0 \to \infty$, the barotropic mode is in a state of no motion where the wind is balanced by the longshore pressure gradient, $p_{0x} = -(u_*^2/h_n)\theta(a - |x|)$.

The first terms in (28a, c) describe a coastal jet within the wind patch. The remaining terms are due to coastal Kelvin waves which have radiated from the wind edges with the coast to the right. In the stationary case these waves are pure damped ones. The associated damping rates, $\lambda_n r$, depend on the vertical mode number, i.e., the higher modes are stronger affected. In particular the very high modes are close to a coastal jet regime while the lower ones are substantially influenced by the Kelvin waves.

In order to illustrate the effects of the Kelvin waves we consider the case $r \to 0$, where the set (28) reduces to

$$u_n(x, y) = -\frac{u_*^2}{fh_n} \frac{e^{-y/R_n}}{R_n} [\theta(a - |x|)(x + a) + \theta(x - a)2a] \tag{29a}$$

$$v_n(x, y) = \frac{u_*^2}{fh_n} \theta(a - |x|)(1 - e^{-y/R_n}) \tag{29b}$$

$$p_n(x, y) = -\frac{u_*^2}{h_n} e^{-y/R_n}[\theta(a - |x|)(x + a) + \theta(x - a)2a] \tag{29c}$$

$$w_n(x, y) = 0. \tag{29d}$$

From this set it can be seen that the Kelvin waves arrest the coastal jet and stop the upwelling. Close to the coast, $y = 0$, the wind is balanced by the alongshore pressure gradient p_{nx}.

A further important effect is the generation of an undercurrent which becomes visible after performing the vertical mode summation. Introducing the sum

$$S_3(y, z) = H_{\text{mix}} \sum_{n=1}^{\infty} \frac{F_n(z)e^{-y/R_n}}{h_n R_n}$$

$$= \frac{2}{R_1\pi} \sum_{n=1}^{\infty} \sin\left(\frac{n\pi H_{\text{mix}}}{H}\right) \cos\left(\frac{n\pi z}{H}\right) e^{-ny/R_1}$$

$$= \frac{1}{R_1\pi}\left[\frac{\sin\varphi_+}{\cosh(y/R_1) - \cos\varphi_+} + \frac{\sin\varphi_-}{\cosh(y/R_1) - \cos\varphi_-}\right] \tag{30}$$

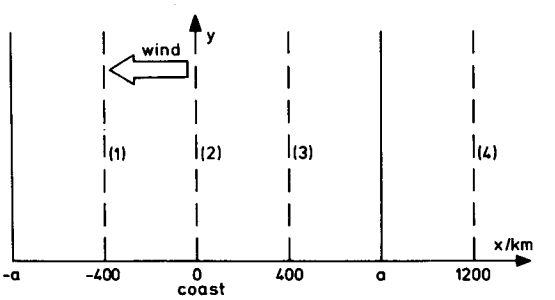

FIG. 4. A schematic diagram showing the position of the ocean boundary, the structure of the wind field, and the location of sections (1) to (4). The wind stress is negative and yields a friction velocity, u_*^2, of 0.5 cm^2 s^{-2}. The value of a is 800 km.

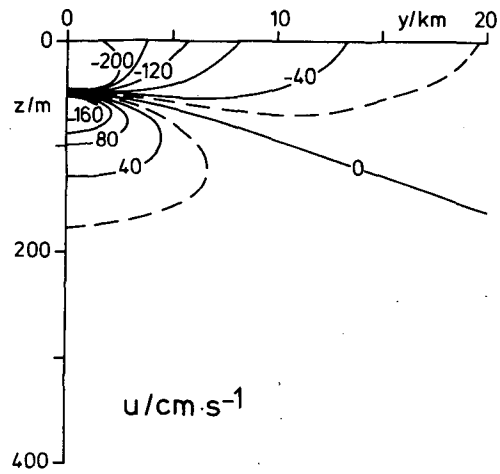

FIG. 5. Vertical section of the longshore current along section (2) of Fig. 4 in the inviscid case showing the arrested coastal jet in the surface layer and an undercurrent below. Close to the point $y = 0$, $z = -H_{mix}$ a singularity occurs. The contour interval is 40 cm s^{-1}.

and using (25a), we obtain

$$u(x, y, z) = -\frac{u_*^2}{fH_{mix}} \times [(x + a)\theta(a - |x|) + 2a\theta(a - x)]S_3(y, z) \quad (31a)$$

$$v(x, y, z) = -\frac{X}{f} + \frac{u_*^2}{fH_{mix}} S_1(0, y, z) \quad (31b)$$

$$p(x, y, z) = -\frac{u_*^2}{H_{mix}} \times [(x + a)\theta(a - |x|) + 2a\theta(a - x)]S_1(0, y, z). \quad (31c)$$

The longshore current consists of an arrested surface jet and an undercurrent below, both are coastally trapped, as displayed in Fig. 5. For $y = 0$ and $z = -H_{mix}u$ becomes singular, i.e., the inviscid solution fails in the vicinity of that point.

The dynamical balance is governed by

- within the patch, $-a < x < a$:

$$-fv + p_x = X$$
$$fu + p_y = 0$$
$$u_x + v_y = 0 \quad (32)$$

- outside the patch, $x > a$:

$$fu + p_y = 0.$$

There is no upwelling in the inviscid solution and the offshore Ekman flow supplies the coastal undercurrent.

In the viscid case the lower modes are in a balance close to (32) while the higher modes approach the balance (27). Thus, due to the strong damping of the Kelvin waves associated with higher vertical modes the upwelling is small but not zero. In other words, adding mixing allows upwelling to occur.

With (25a, b) we find the final solution as

$$u(x, y, z) = -\frac{u_*^2}{rH_{mix}} [\theta(a - |x|)S_1(0, y, z) - \theta(x + a)S_1(x + a, y, z) + \theta(x - a)S_1(x - a, y, z)] \quad (33a)$$

$$v(x, y, z) = -\frac{X}{f} - \frac{u_*^2}{fH_{mix}} S_1(0, y, z) \quad (33b)$$

$$w(x, y, z) = \frac{u_*^2}{NH_{mix}} [\theta(a - |x|)S_2(0, y, z) - \theta(x + a)S_2(x + a, y, z) + \theta(x - a)S_2(x - a, y, z)]. \quad (33c)$$

We choose $a = 800$ km and the other parameters as in the foregoing subsection. In Figs. 6 to 9 the longshore velocity (33a) is displayed along the sections (1) to (4), respectively, which are indicated in Fig. 4. The flow compares well with that of McCreary's model, and has features that compare favorably with those observed, see McCreary (1981) and references therein.

Both the thickness and the depth of the undercurrent increase with increasing distance from the wind edge $x = -a$. Due to the radiation of the Kelvin waves the coastal currents extend well outside the wind band, $x > a$, where they are remotely driven by the winds blowing within the forcing area.

Figure 10 shows the vertical velocity (33c) along section (2) as indicated in Fig. 4, and demonstrates the

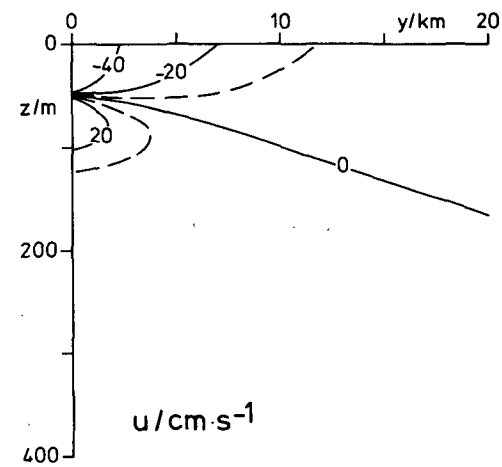

FIG. 6. Vertical section of the longshore current in the viscid case showing the arrested coastal jet and the undercurrent along section (1) of Fig. 4. The contour interval is 20 cm s^{-1}.

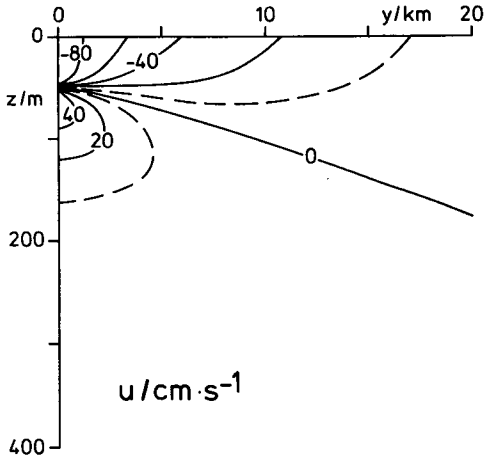

FIG. 7. As in Fig. 6, but along section (2) of Fig. 4.

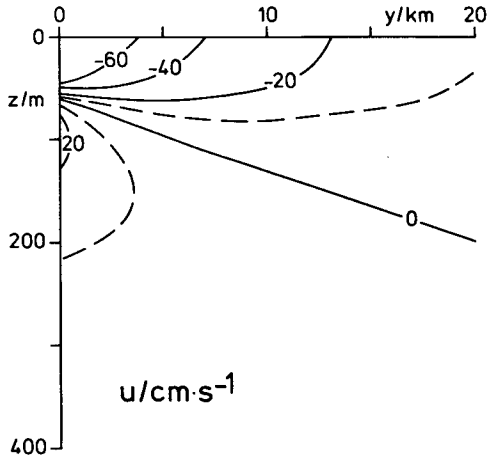

FIG. 9. As in Fig. 6, but along section (4) of Fig. 4.

reduction of the upwelling compared with that of the coastal jet case shown in Fig. 3. The cross velocity is not affected by the Kelvin waves and has within the wind band the same structure as depicted in Fig. 2.

The dependence of the longshore current profile close to the coast on the parameter r and on the mixed layer depth H_{mix} is illustrated in Figs. 11 and 12. The profile appears to be relative sensitive to changes in r and H_{mix}. The sensitive dependence on r close to the coast corresponds to the singularity of u at $y = 0$ and $z = -H_{\text{mix}}$ which occurs in the inviscid case, $r \to 0$. Further offshore the properties of the flow are only weakly affected by changes in r.

Just for completeness we note also the solutions far offshore. For $y/R_1 \gg 1$ from (20) we obtain

$$G_n * 1 = \frac{-R_n^2}{1 + k^2 R_n^2}, \quad G_{ny} * 1 = 0.$$

Inserting this into (19) we find after inverse Fourier transforms

$$u_n = 0$$

$$v_n(x) = \frac{u_*^2}{f h_n}\left[\theta(a - |x|) + \operatorname{sgn}(x - a)\frac{e^{-|x-a|/R_n}}{2} - \operatorname{sgn}(x + a)\frac{e^{-|x+a|/R_n}}{2}\right]$$

$$p_n(x) = -\frac{u_*^2}{h_n \lambda_n}\left[\frac{e^{-|x-a|/R_n}}{2} - \frac{e^{-|x+a|/R_n}}{2}\right]$$

$$w_n = 0$$

where orders of r/f have been neglected. For v the mode sum can be carried out, i.e.,

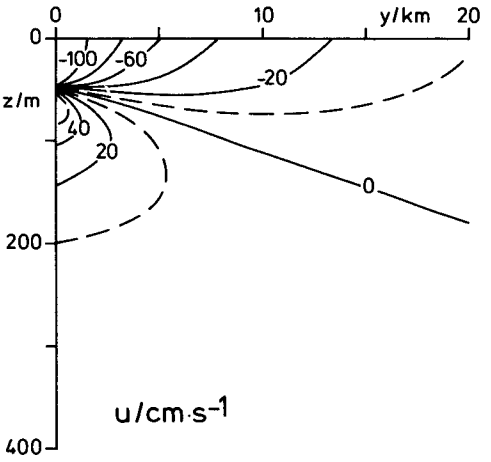

FIG. 8. As in Fig. 6, but along section (3) of Fig. 4.

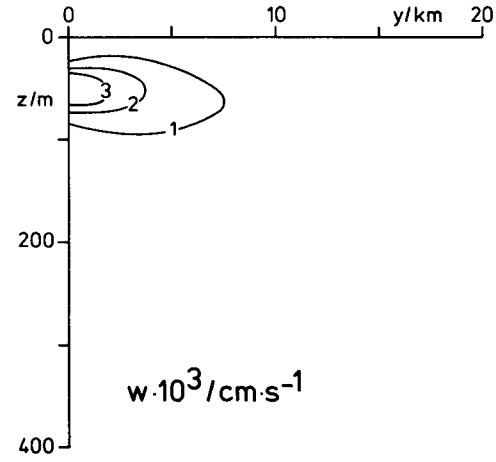

FIG. 10. Vertical section of the vertical velocity along section (2) of Fig. 4. Contour interval is 10^{-3} cm s^{-1}. Velocity is multiplied by 10^3.

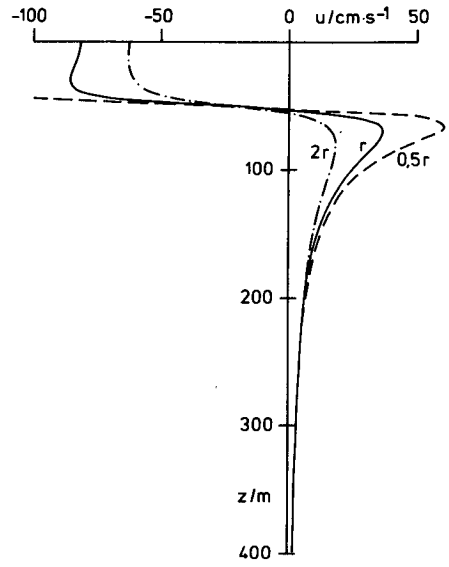

FIG. 11. Profiles of the longshore current close to the coast at section (2) of Fig. 4, contrasting the response for three different values of the dissipation constant. The value of r is (30 days)$^{-1}$.

$$v(x, z) = \frac{-X}{f} + \frac{u_*^2}{2fH_{\text{mix}}}\left[\text{sgn}(x-a)S_1(|x-a|, 0, z) - \text{sgn}(x+a)S_1(|x+a|, 0, z)\right]. \quad (34)$$

Thus, far offshore the response consists of the Ekman flow (first term) and a rectification at the edges of the wind band (second term). This rectification is geostrophically balanced by the pressure gradient p_x.

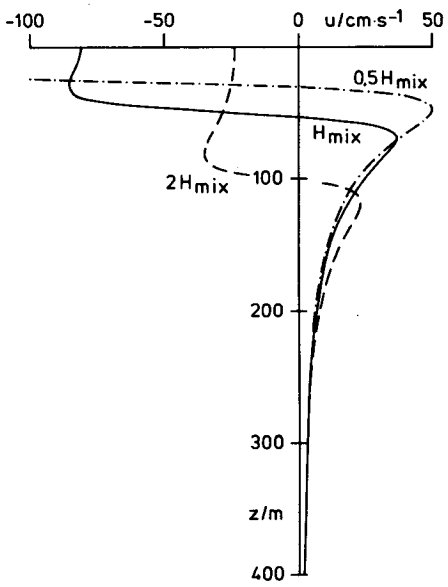

FIG. 12. Profiles of the longshore current close to the coast at section (2) of Fig. 4, contrasting the response for three different values of mixed layer depth. The value of H_{mix} is 50 m.

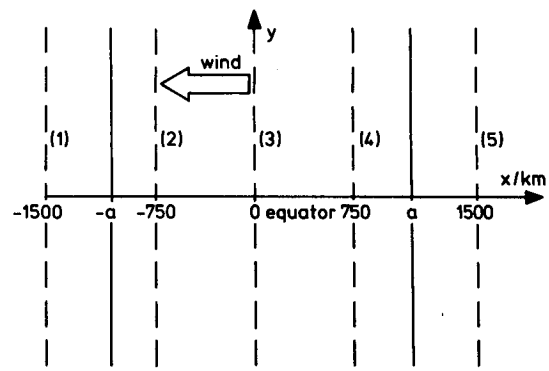

FIG. 13. A schematic diagram showing the structure of the zonal wind band and the locations of sections (1) to (5). The wind blows in negative zonal direction. The friction velocity, u_*^2, is 0.25 cm^2 s^{-2} and the value of a is 1000 km.

5. Response of an unbounded equatorial ocean

In this section we consider the stationary response of an unbounded equatorial ocean to a zonal wind patch of the width $2a$ as given by (20a, b), compare Fig. 13. The algebra is much more complicated than in the coastal case discussed in the previous section and closed form expressions of the final solution can be obtained only in very few cases.

Inserting (18) into the formal solution (16) and using (17b) we obtain the corresponding response as

$$u_n = -\frac{u_*^2}{h_n} 2\pi\delta(\omega)\frac{2\sin ka}{k}\frac{1}{r^2\lambda_n^2 + k^2} \times [r\lambda_n^2(1 + \lambda_n^2\beta^2 y G_n * y') + ik\beta\lambda_n^2 G_{ny} * y']$$

$$v_n = -\frac{u_*^2}{h_n} 2\pi\delta(\omega)\frac{2\sin ka}{k}\lambda_n^2\beta G_n * y'$$

$$p_n = -\frac{u_*^2}{h_n} 2\pi\delta(\omega)\frac{2\sin ka}{k}\frac{-i}{r^2\lambda_n^2 + k^2} \times [k(1 + \lambda_n^2\beta^2 y G_n * y') - ir\lambda_n^2\beta G_{ny} * y']. \quad (35)$$

Due to the delta function all ω occurring in the solution vanish. In the following we omit the vertical mode index n and only retain it when discussing the vertical mode sums. Next we calculate the convolution $G_n * y'$. Introducing a new variable $\eta = \sqrt{\lambda\beta}y$ we have

$$G_n * y' = \int_{-\infty}^{+\infty} G(y, y')y'dy' = \int_{-\infty}^{+\infty} G(\eta, \eta')\eta'\frac{d\eta'}{\lambda\beta} = \frac{1}{\sqrt{\lambda\beta}}\sum_{m=0}^{\infty}\frac{\psi_m(\eta)}{-(r^2\lambda^2 + k^2) + \frac{i\beta}{r}k - \beta\lambda(2m+1)} \times \int_{-\infty}^{+\infty} d\eta'\eta'\psi_m(\eta') \quad (36)$$

where $(\lambda\beta)^{-1} = R$ defines the equatorial Rossby radius.

The integral in (36) yields only for odd m nonzero contributions, i.e.,

$$\int_{-\infty}^{+\infty} d\eta' \eta' \psi_{2m+1}(\eta') = I_{2m}\sqrt{4m+2}$$

with

$$I_{2m} = \frac{\pi^{1/4}\sqrt{2(2m)!}}{m!2^m}.$$

Note that I_{2m} is the coefficient of the expansion

$$\sum_{m=0}^{\infty} I_{2m}\psi_{2m}(\eta) = 1. \tag{37}$$

We may write the denominator of (36) as

$$r^2\lambda^2 + k^2 - i\beta\frac{k}{r} + \lambda\beta(2m+1) = (k - ik_1)(k + ik_2)$$

where

$$k_{1,2} = \frac{\beta}{2r}\left[\left(1 + 4r^2\frac{\lambda}{\beta}(2m+1)\right)^{1/2} \pm 1\right].$$

For small r it follows $k_1 \approx \beta/r$ and $k_2 \approx r\lambda(2m+1)$, which correspond to damped eastward propagating short Rossby waves and westward propagating long Rossby waves, respectively. Thus, with

$$G * y' = -\frac{1}{\sqrt{\lambda\beta}}\sum_{m=0}^{\infty}\frac{I_{2m}\sqrt{4m+2}\psi_{2m+1}(\eta)}{(k - ik_1)(k + ik_2)}$$

from (35) we obtain

$$u = -\frac{u_*^2}{h}\frac{2\sin ka}{k}\frac{r\lambda^2}{r^2\lambda^2 + k^2} \times\left[1 - \lambda\beta\sum_{m=0}^{\infty}\frac{I_{2m}\sqrt{4m+1}}{(k - ik_1)(k + ik_2)} \times\left(\eta\psi_{2m+1}(\eta) + \frac{ik}{r\lambda}\psi_{2m+1}(\eta)\right)\right]$$

$$v = \frac{u_*^2}{h_n}\frac{2\sin ka}{k}\sqrt{\lambda\beta}\sum_{m=0}^{\infty}\frac{I_{2m}\sqrt{4m+2}\psi_{2m+1}(\eta)}{(k - ik_1)(k + ik_2)}$$

$$p = -\frac{u_*^2}{h_n}\frac{2\sin ka}{k}\frac{ik}{r^2\lambda^2 + k^2} \times\left[1 + \lambda\beta\sum_{m=0}^{\infty}\frac{I_{2m}\sqrt{4m+2}}{(k - ik_1)(k + ik_2)}\left(\eta\psi_{2m+1}(\eta) + \frac{ir\lambda}{k}\psi'_{2m+1}(\eta)\right)\right]. \tag{38}$$

The inverse Fourier transforms with respect to k can be performed exactly.

Introducing

$$\Lambda_0(x) = \int\frac{dk}{2\pi}\frac{2\sin ka}{k}\frac{e^{ikx}}{k^2 + r^2\lambda^2} = \frac{1}{r^2\lambda^2}\left[\theta(a - |x|) + \operatorname{sgn}(x - a)\frac{e^{-r\lambda|x-a|}}{2} - \operatorname{sgn}(x + a)\frac{e^{-r\lambda|x+a|}}{2}\right]$$

and

$$\Lambda_1(x) = \int\frac{dk}{2\pi}\frac{2\sin ka}{k}\frac{e^{ikx}}{(k^2 + r^2\lambda^2)(k - ik_1)(k + ik_2)} = \frac{\theta(a - |x|)}{k_1k_2r^2\lambda^2} + \frac{1}{k_1(k_1 + k_2)(r^2\lambda^2 - k_1^2)}$$

$$\times[\theta(x - a)e^{-k_1(x-a)} - \theta(x + a)e^{-k_1(x+a)}] + \frac{1}{k_2(k_1 + k_2)(r^2\lambda^2 - k_2^2)}[\theta(a - x)e^{-k_2(a-x)} - \theta(-a - x)e^{k_2(a+x)}]$$

$$- \frac{1}{2(r\lambda)^2(r\lambda - k_1)(r\lambda + k_2)}[\theta(x - a)e^{-r\lambda(x-a)} - \theta(x + a)e^{-r\lambda(x+a)}] + \frac{1}{2(r\lambda)^2(r\lambda + k_1)(r\lambda + k_2)}[\theta(a - x)e^{-r\lambda(a-x)} - \theta(-x - a)e^{r\lambda(x+a)}],$$

all Fourier integrals occurring in (38) can be expressed by Λ_0 and Λ_1. For simplicity we use the approximations $k_1 \approx \beta/r$ and $k_2 \approx r\lambda(2m+1)$. Moreover we ignore the short Rossby wave contributions which appear to be closely trapped at the edges of the wind patch. These assumptions amount to the usual long-wavelength approximation. Then we obtain

$$u(x,\eta) = -\frac{u_*^2}{rh}\Bigg\{\overbrace{\theta(a - |x|)\left(1 - \sum_{m=0}^{\infty} I_{2m}\frac{4m+2}{4m+3}\eta\psi_{2m+1}(\eta)\right)}^{\text{Yoshida}} + \overbrace{\frac{I_0}{2}\psi_0(\eta)[\theta(x - a)e^{-r\lambda(x-a)} - \theta(x + a)e^{-r\lambda(x+a)}]}^{\text{Kelvin}}$$

$$+ \overbrace{\sum_{m=0}^{\infty}\frac{1}{2(4m+3)}(I_{2m+2}\psi_{2m+2} - I_{2m}\psi_{2m})(\theta(a - x)e^{-r\lambda(4m+3)(a-x)} - \theta(-a - x)e^{r\lambda(4m+3)(a+x)})}^{\text{Rossby}}\Bigg\} \tag{39a}$$

$$v(x,\eta) = -\frac{u_*^2}{h}\left(\frac{\lambda}{\beta}\right)^{1/2} \sum_{m=0}^{\infty} \frac{I_{2m}\sqrt{4m+2}}{4m+3}\psi_{2m+1}(\eta)[\theta(a-|x|) - \theta(a-x)e^{-r\lambda(4m+3)(a-x)} + \theta(-a-x)e^{r\lambda(4m+3)(x+a)}] \quad (39b)$$

$$p(x,\eta) = -\frac{u_*^2}{rh\lambda}\left\{\theta(a-|x|)\sum_{m=0}^{\infty}\frac{1}{(4m+3)}(2(m+1)I_{2m+2}\psi_{2m+2} - (2m+1)I_{2m}\psi_{2m}) - \frac{I_0}{2}\psi_0(\eta)[\theta(x-a)e^{-r\lambda(x-a)} - \theta(x+a)e^{-r\lambda(x+a)}] - \sum_{m=0}^{\infty}\frac{1}{2(4m+3)}(I_{2m+2}\psi_{2m+2} + I_{2m}\psi_{2m}) \times (\theta(a-x)e^{-r\lambda(4m+3)(a-x)} - \theta(-a-x)e^{r\lambda(4m+3)(x+a)})\right\} \quad (39c)$$

where standard identities of the Hermite functions were used. The first terms in (39a, c) describe the Yoshida jet within the forcing area, see, e.g., Moore and Philander (1977), while the second and third terms are due to eastward propagating Kelvin waves and westward propagating long Rossby waves, respectively, which are excited at the edges of the wind patch. Clearly, in the steady state considered here these waves are purely damped ones. The damping rate of the Kelvin is $r\lambda$, that of the Rossby waves, however, appears to be proportional to both the vertical eigenvalue and to the meridional mode number as $r\lambda(4m+3)$.

In the remainder of this section we discuss the solution (39), particularly the zonal current in some detail.

a. Yoshida jet

We start with the case of an unlimited wind field, i.e., $a \to \infty$. Then in the set (39) all exponentials due to Kelvin and Rossby waves vanish and only the Yoshida terms remain. The resulting balances are quite similar to those of the coastal jet regime, compare (27)

$$ru - \beta yv = X$$

with $ru = X$ for $y = 0$, $-\beta yv = X$ for $y \to \infty$.

$$\beta yu + p_y = 0$$
$$v_y + w_z = 0 \quad (40)$$

where $rv \ll \beta yu$ was assumed.

We try to find a closed form expression of the zonal current, i.e., the Yoshida jet. This requires an analytically tractable approximation to the involved infinite series of Hermite function. To this end we note that the expansion (37) can be rearranged as

$$\sum_{m=0}^{\infty} I_{2m}\psi_{2m}(\eta) = \psi_0(\eta)\sum_{m=0}^{\infty}\left[\frac{I_{2m}H_{2m}(0)}{2^m\sqrt{(2m)!}} + \frac{I_{2m}(H_{2m}(\eta) - H_{2m}(0))}{2^m\sqrt{(2m)!}}\right] = 1.$$

With

$$H_{2m}(0) = (-1)^m\frac{(2m)!}{m!}$$

it can readily be seen that the sum

$$\frac{1}{\pi^{1/4}}\sum_{m=0}^{\infty}\frac{I_{2m}H_{2m}(0)}{2^m\sqrt{(2m)!}}$$

is the Taylor series of $[2/(1+x)]^{1/2}$ for $x = 1$, which converges in the interval $-1 < x \leqslant 1$. Thus, we have

$$e^{-\eta^2/2} + \psi_0(\eta)\sum_{m=0}^{\infty}\frac{I_{2m}(H_{2m}(\eta) - H_{2m}(0))}{2^m\sqrt{(2m)!}} = 1.$$

The sum over $\eta\psi_{2m+1}(\eta)$ occurring in the Yoshida term in (39a) can be rearranged analogously. Using the recurrence relations of Hermite functions we obtain

$$\sum_{m=0}^{\infty}\frac{I_{2m}\sqrt{4m+2}}{4m+3}\eta\psi_{2m+1}(\eta) = \psi_0(\eta)\sum_{m=0}^{\infty}\frac{I_{2m}(H_{2m}(\eta) - H_{2m}(0))}{2^m\sqrt{(2m)!}} \times\left(\frac{2m+1}{4m+3} + \frac{2m}{4m-1}\right).$$

Hence the Yoshida term in (39a) can be rewritten as

$$u = \frac{-u_*^2}{rh}\left[e^{-\eta^2/2} - \psi_0(\eta)\sum_{m=0}^{\infty}\frac{I_{2m}(H_{2m}(\eta) - H_{2m}(0))}{2^m\sqrt{(2m)!}} \times\frac{2}{(4m+3)(4m-1)}\right]. \quad (41)$$

It appears that for $\eta < 2$ the sum is negligible. For $\eta > 2$ both terms are of the same order but the resulting signal is rather weak, say less than 10 percent compared with the values close to the equator. Consequently, the exponential yields the leading contribution to the Yoshida jet. A comparison of the complete contribution of the bracket of (41) with its approximation by the first term is depicted in Fig. 14.

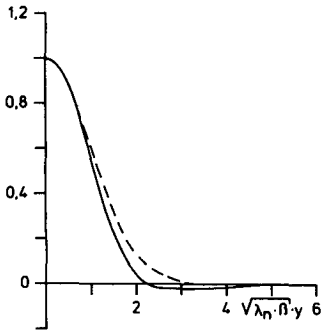

FIG. 14. Comparison of the infinite series of Hermite functions in the bracket of (41) (solid curve) with the approximate expression, $\exp(-\eta^2/2)$, (dashed curve).

Retaining the vertical mode index n, we have

$$u_n(y) \approx -\frac{u_*^2}{rh_n} e^{-\eta_n^2/2}.$$

Note that $\eta_n = \sqrt{\lambda_n \beta} y = \sqrt{n} y/R_1$, *where* R_1 is the baroclinic equatorial Rossby radius. Hence, with the aid of (25a) the vertical mode summation can easily be performed

$$u(y, z) = -\frac{u_*^2}{rH_{\text{mix}}}\left[\tilde{S}_1(0, y, z) + \frac{H_{\text{mix}}}{H}\right]. \quad (42)$$

The tilde indicates that in the equatorial case the y/R_1 occurring in S_1 has to be replaced by $y^2/2R_1{}^2$, i.e.,

$$\tilde{S}_1(0, y, z) = \frac{1}{\pi}\left[\arctan\left(\frac{\sin\varphi_+}{e^{y^2/2R_1{}^2} - \cos\varphi_+}\right) + \arctan\left(\frac{\sin\varphi_-}{e^{y^2/2R_1} - \cos\varphi_-}\right)\right]. \quad (43)$$

The Yoshida jet as given by (42) is shown in Fig. 15, where the involved parameters have been chosen as H = 4000 m, H_{mix} = 75 m, λ_1 = 0.36 s m, R_1 = 360 km, u_*^2 = ¼ cm^2 s^{-2}, and r^{-1} = 90 days. The jet is confined to the surface layer and has a maximum amplitude of 250 cm s^{-1}; its magnitude is proportional to r^{-1} and H_{mix}^{-1}.

Similarly to the coastal jet case the associated vertical velocity has a logarithmic singularity at $y = 0$ and $z = -H_{\text{mix}}$. This follows from (39c) and (4). In the two-dimensional case only the first sum in the braces of (39c) contributes to p_n. For $y = 0$ this sum is of order unity and the vertical mode summation according to (4) is proportional to $S_2(0, 0, z)$, compare (25b).

Such a singularity does not occur in the Yoshida jet solution of McCreary (1981a), i.e., using heat diffusion rather Newtonian cooling removes the singularity. However, McCreary's two-dimensional solution yields speeds that are too high.

b. Equatorial undercurrent

Next we consider the response to the finite wind band as given by (39). First we note that because of the rigid-lid condition, implying $\lambda_0 \to 0$, the barotropic mode is in Sverdrup balance, which in the present case is a state of rest where the pressure gradient balances the wind.

The baroclinic Kelvin and Rossby waves are expected to have two effects, namely, to arrest the Yoshida jet and to introduce an undercurrent. Again this can be seen easiest in the inviscid case, $r \to 0$, where the set (39) reduces to

$$u_n = -\frac{u_*^2}{h_n} I_0\psi_0(\eta_n)\frac{a}{\beta R_n{}^2}$$

$$p_n = -\frac{u_*^2}{h_n}[aI_0\psi_0(\eta_n) - (a - x)\theta(a - |x|) - 2a\theta(-x - a)]$$

$$v_n = w_n = 0. \quad (44)$$

The dynamical balance is simply

$$p_{nx} = -\frac{u_*^2}{h_n}\theta(a - |x|)$$

$$\beta y u_n + p_{ny} = 0. \quad (45)$$

Thus, similarly to the coastal ocean response, the surface jet is arrested by the eastward propagating Kelvin waves and, moreover, by the westward propagating long Rossby waves. The upwelling has stopped completely. Contrary to the inviscid coastal ocean, the zonal current is independent of x and the meridional current vanishes. Within the wind band the zonal pressure gradient balances the wind, and the zonal current is geostrophically adjusted to the meridional pressure gradient.

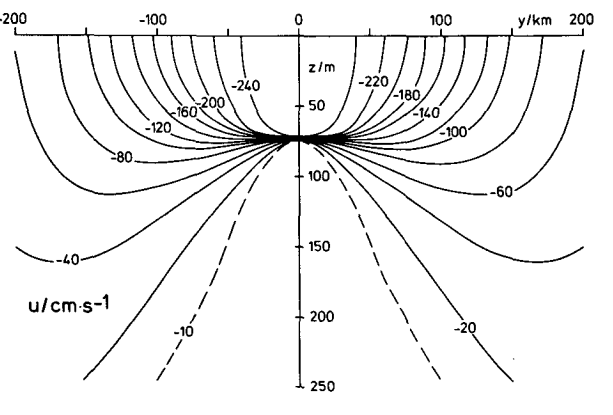

FIG. 15. Vertical section of the Yoshida jet. The contour interval is 20 cm s^{-1}. The maximum speed at the equator is about 250 cm s^{-1}.

The generation of an undercurrent can be demonstrated after summing up the vertical modes. With the aid of (25a), (30) and (7) we obtain

$$u(y, z) = -\frac{u_*^2}{H_{\text{mix}}}\frac{a}{\beta R_1}\tilde{S}_3(y, z) \tag{46}$$

where

$$\tilde{S}_3(y, z) = \frac{1}{\pi R_1}\left[\frac{\sin\varphi_+}{\cosh(y^2/2R_1^2) - \cos\varphi_+} + \frac{\sin\varphi_-}{\cosh(y^2/2R_1^2) - \cos\varphi_-}\right] \tag{47}$$

$$p(y, z) = -\frac{u_*^2}{H_{\text{mix}}}\{a\tilde{S}_1(0, y, z) - [(a - x)\theta(a - |x|) + 2a\theta(-x - a)]\theta(z + H_{\text{mix}})\}. \tag{48}$$

The zonal current is shown in Fig. 16. Beneath the westward surface jet flows an undercurrent. Close to the point $y = 0$ and $z = -H_{\text{mix}}$ this solution becomes singular. This follows from the behavior of the vertical mode sum at $y = 0$, i.e.,

$$u(0, z) = \frac{u_*^2}{H_{\text{mix}}}\frac{a2}{\beta R_1 \pi}\sum_{n=1}^{\infty}\sin\left(\frac{n\pi H_{\text{mix}}}{H}\right)\cos\left(\frac{n\pi z}{H}\right).$$

Note that this sum is singular only if the summation goes really over all infinite n. If the sum would be truncated at some finite n the result remains finite.

For nonzero damping rate there will establish a combination of both regimes (40) and (45), in particular, the very high modes are close to the Yoshida regime (40) while the lower modes approach the balance (45).

In order to find a closed form expression of the zonal current for nonzero r we have to seek also a mathematically convenient approximation of the Hermite series occurring in the Rossby wave contribution in (39a). To this end we note that the Yoshida jet term in (39a), which according to (41) can be approximated by $e^{-\eta^2/2}$, can be rewritten as

$$1 - \sum_{m=0}^{\infty} I_{2m}\frac{\sqrt{4m+2}}{4m+3}\eta\psi_{2m+1}(\eta) = \frac{I_0\psi_0(\eta)}{2} + \frac{1}{2}\sum_{m=0}^{\infty}\frac{1}{4m+3}(I_{2m+2}\psi_{2m+2} - I_{2m}\psi_{2m}) \approx e^{-\eta^2/2}.$$

This implies

$$\frac{1}{2}\sum_{m=0}^{\infty}\frac{1}{4m+3}(I_{2m+2}\psi_{2m+2} - I_{2m}\psi_{2m}) \approx \frac{1}{\sqrt{2}}(\sqrt{2} - 1)e^{-\eta^2/2}. \tag{49}$$

This result follows also if the $\psi_{2m}(\eta)$ are replaced by

$$\psi_0(\eta)\frac{H_{2m}(0)}{2^m\sqrt{(2m)!}}.$$

Thus, similar as in the Yoshida case, we can approximate the Rossby terms by taking only the $\eta = 0$ values of the Hermite polynomials into account.

Let $\xi = e^{-r\lambda(a-x)}$ and consider the series

$$\frac{\psi_0}{2}\sum_{m=0}^{\infty}\frac{\xi^{4m+3}}{4m+3}\left[\frac{I_{2m+2}}{2^{m+1}\sqrt{(2m+2)!}}H_{2m+2}(0) - \frac{I_{2m}}{2^m\sqrt{(2m)!}}H_{2m}(0)\right]$$
$$= \frac{e^{-\eta^2/2}}{\sqrt{2}\xi}\sum_{m=0}^{\infty}\frac{(\xi^4)^{m+1}(2m)!(-1)^{m+1}}{2^{2m+1}(m+1)!m!}$$
$$= \frac{e^{-\eta^2/2}}{\sqrt{2}}\cdot\frac{1}{\xi}(1 - \sqrt{1+\xi^4}). \tag{50}$$

For $\xi = 1$ this yields again (49). Thus with (50) the sum over m in the approximate Rossby term can be written as

$$\frac{\psi_0(\eta)}{2}\sum_{m=0}^{\infty}\frac{1}{4m+3}\left(\frac{I_{2m+2}H_{2m+2}(0)}{2^{m+1}\sqrt{(2m+2)!}} - \frac{I_{2m}H_{2m}(0)}{2^m\sqrt{(2m)!}}\right) \times [\theta(a - x)e^{-r\lambda_n(4m+3)(a-x)} - \theta(-a - x)e^{r\lambda_n(4m+3)(a+x)}]$$
$$= \frac{e^{-\eta^2/2}}{\sqrt{2}}\{\theta(a - x)e^{r\lambda_n(a-x)}[1 - (1 + e^{-4r\lambda_n(a-x)})^{1/2}] - \theta(-a - x)e^{-r\lambda_n(a+x)}[1 - (1 + e^{4r\lambda_n(a+x)})^{1/2}\}. \tag{51}$$

Unfortunately, with (51) the vertical mode sum cannot be performed without further simplification. However, it turns out that (50), and hence (51), can be well approximated by the first two terms of its Taylor expansion, i.e.,

$$-\frac{1}{\xi}(1 - \sqrt{1+\xi^4}) \approx \frac{\xi^3}{2} - \frac{\xi^7}{8}.$$

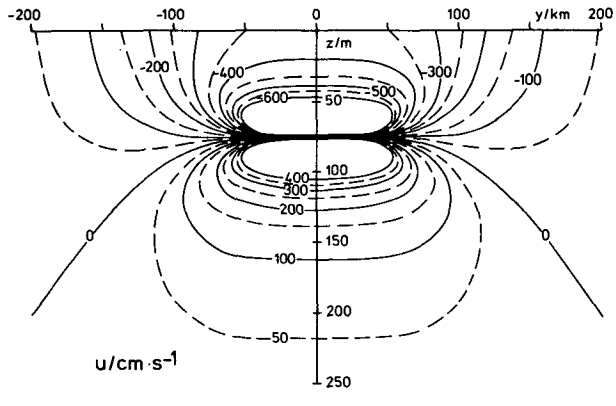

FIG. 16. Vertical section of the zonal current in the inviscid case showing an eastward undercurrent below a westward surface flow (arrested Yoshida jet). Similarly to the coastal ocean response in Fig. 5 the neglect of friction causes a singularity at $y = 0$ and $z = -H_{\text{mix}}$.

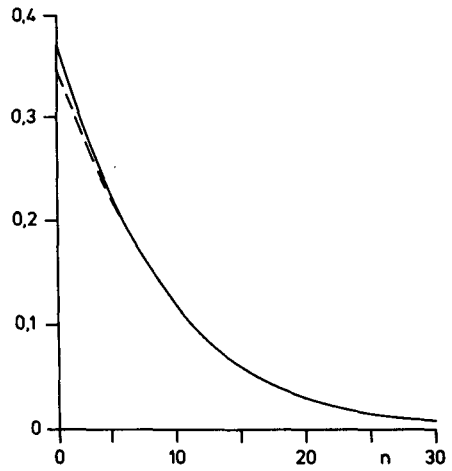

FIG. 17. Comparison of the exact Rossby term at the equator, $y = 0$, (solid line), and the approximate expression (52), which consists of the first two meridional modes (dashed line) versus the vertical mode number. The involved parameters are chosen as $\lambda_1 = 0.36$ s m, $1/r = 90$ days, $a = 1000$ km and $x = 0$.

This approximation is accurate for vertical modes $n \geq 4$. For the first few modes the error is also small, say, of the order of few percent. Thus we can replace (51) by

$$-\frac{e^{-\eta^2/2}}{\sqrt{2}}\left[\theta(a-x)\left(\frac{e^{-3r\lambda_n(a-x)}}{2}-\frac{e^{-7r\lambda_n(a-x)}}{8}\right)\right.$$
$$\left.-\theta(-a-x)\left(\frac{e^{3r\lambda_n(a+x)}}{2}-\frac{e^{7r\lambda_n(a+x)}}{8}\right)\right]. \quad (52)$$

Figure 17 compares the approximate formula (52) with the complete expression (51). We observe that the expressions drop rather rapidly with increasing mode number n. This is due to the enhanced damping rate of the long Rossby waves, i.e., the occurrence of the factor $(4m + 3)$ in the corresponding exponentials. Clearly, the Kelvin as well as the Yoshida terms converge significantly slower.

With (52) and the approximation of the Yoshida term discussed in the previous subsection we have (39a) simplified to

$$u_n(x, y) = -\frac{u_*^2}{rh_n}\left\{\theta(a-|x|)e^{-\eta_n^2/2}+\frac{e^{-\eta_n^2/2}}{\sqrt{2}}\right.$$
$$\times\left(\theta(x-a)e^{-r\lambda_n(x-a)}-\theta(x+a)e^{-r\lambda_n(x+a)}\right)$$
$$-\frac{e^{-\eta_n^2/2}}{\sqrt{2}}\left[\theta(a-x)\left(-\frac{e^{-3r\lambda_n(a-x)}}{2}+\frac{e^{-7r\lambda_n(a-x)}}{8}\right)\right.$$
$$\left.\left.-\theta(-a-x)\left(-\frac{e^{3r\lambda_n(a+x)}}{2}+\frac{e^{7r\lambda_n(a+x)}}{2}\right)\right]\right\}$$

Now the corresponding vertical mode sums can be expressed by $\tilde{S}_1$ and we find the final solution as

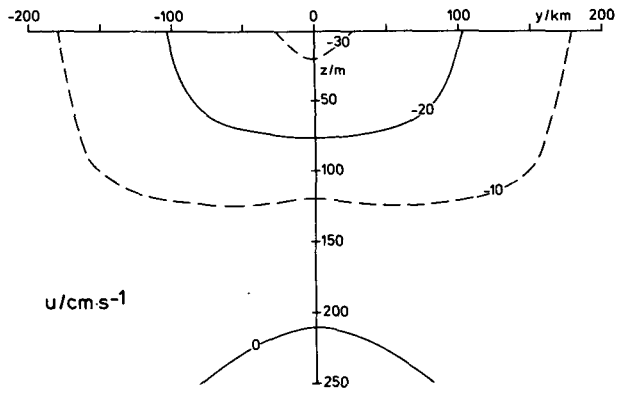

FIG. 18. Vertical section of the zonal current in the viscid case along section (1) of Fig. 13. The contour interval is 20 cm s^{-1}.

$$u(x, y, z) = -\frac{u_*^2}{rH_{\text{mix}}}\left\{\theta(a-|x|)\tilde{S}_1(0, y, z)\right.$$
$$+\frac{1}{\sqrt{2}}\theta(x-a)\tilde{S}_1(x-a, y, z)-\frac{1}{\sqrt{2}}\theta(x+a)$$
$$\times\tilde{S}_1(x+a, y, z)+\theta(a-x)\left[\frac{1}{2\sqrt{2}}\tilde{S}_1[3(a-x), y, z]\right.$$
$$-\frac{1}{8\sqrt{2}}\tilde{S}_1[7(a-x), y, z]\Big]-\theta(-a-x)$$
$$\times\left[\frac{1}{2\sqrt{2}}\tilde{S}_1[-3(a+x), y, z]\right.$$
$$\left.\left.-\frac{1}{8\sqrt{2}}\tilde{S}_1[-7(a+x), y, z]\right]\right\} \quad (53)$$

In Figs. 18 to 22 the zonal current is shown along the sections (1) to (5) as indicated in Fig. 13. The vertical

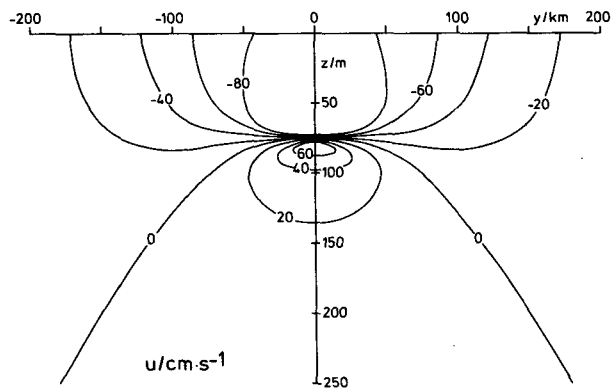

FIG. 19. Vertical section of the zonal current along section (2) of Fig. 13 showing the arrested Yoshida jet in the surface layer and the undercurrent below. The contour interval is 20 cm s^{-1}.

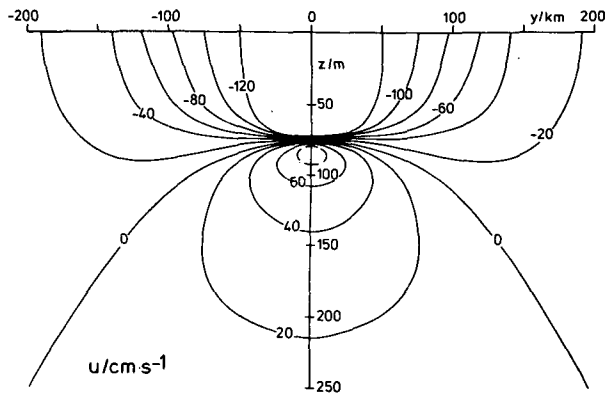

FIG. 20. As in Fig. 19, but along section (3) of Fig. 13.

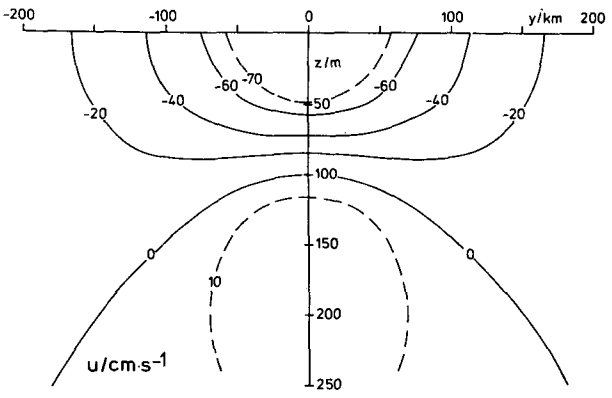

FIG. 22. As in Fig. 19, but along section (5) of Fig. 13.

and meridional scales compare well with observations, particularly within the wind band (see Fig. 19 to 21) however, the surface velocity is somewhat too high.

For an unbounded ocean McCreary (1981a) found in his model a similar ratio of surface velocity to the maximum speed of the undercurrent, compare Fig. 8 of his paper. However, in his case studies he could demonstrate that the effects of meridional boundaries reduce the surface current by about 50 percent and intensifies the undercurrent by a few percent. Thus the relative high surface speed in the present model may be attributed to the neglecting of the boundaries.

McPhaden (1981) obtained a similar figure of the undercurrent but an unrealistically strong surface current, which seems to be due to the lack of a mixed layer in his model.

In Fig. 23 the dependence of the zonal current on the mixed layer depth at $x = 0$, just at the equator is depicted. This figure shows a quite strong variation of the velocity profile as H_{mix} is changed. Thus a mixed layer depth of, say, 75 m is necessary to obtain a reasonable surface speed.

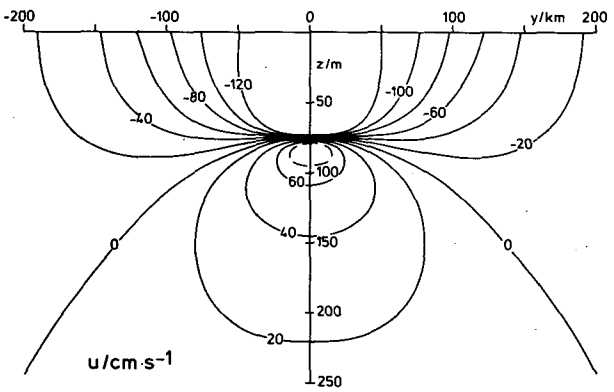

FIG. 21. As in Fig. 19, but along section (4) of Fig. 13.

Figure 24 illustrates how the current profile depends on the friction constant r. Particularly at the equator the current profile appears to be rather sensitive to variations of r, while the meridional and vertical scales are only little affected. Obviously, the sensitivity close to the equator is due to the singularity of u for $r \to 0$, compare Fig. 16.

Figures 23 and 24 reveal that the use of a nonscale specific damping yields a greater shear across the base of the mixed layer than in either McCreary's or McPhaden's models.

6. Summary and discussion

In the paper the wind-driven response of a coastal f-plane ocean and of an unbounded equatorial β-plane ocean was investigated. In section 3 the general formal solutions were derived for both models. The mathe-

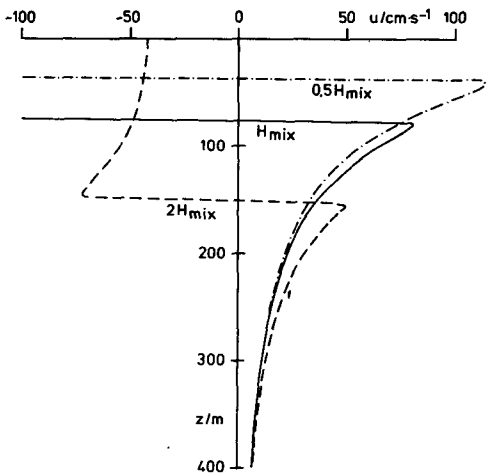

FIG. 23. Profiles of the zonal current at the equator, $y = 0$ and $x = 0$, contrasting the response for three different values of the mixed layer depth. The value of H_{mix} is 75 m.

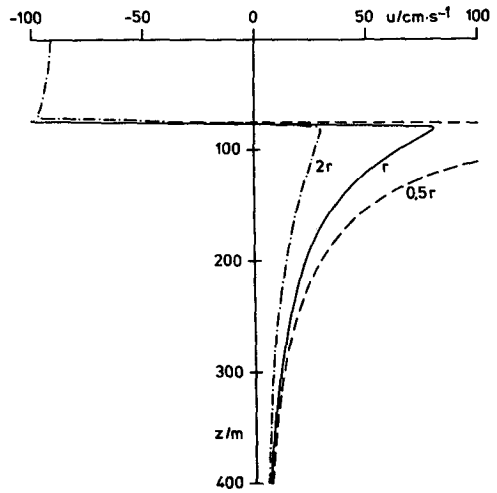

FIG. 24. Profiles of the zonal current at the equator, $y = 0$ and $x = 0$, contrasting the response for three different values of the friction parameter. The value of r is (90 days)$^{-1}$.

matical concept is based on a Green's function technique. The structure of the general solutions are very similar. This indicates a close relationship between the two models, which physically is due to the waveguide properties of a coastal boundary as well as of the equator.

In section 4 the coastal ocean is forced by a steady longshore wind band. The coastal boundary is represented by a vertical wall. Assuming certain simplifications, such as a simple forcing pattern, constant (or weakly varying) Brunt–Väisälä frequency, alongshore geostrophy, and a simple dissipation, the steady state solutions of the current components can be expressed through closed analytical expressions, i.e., the corresponding mode sums are performed explicitly.

Despite of these simplifications the solutions develop a realistic current structure which consists of a downwind surface jet and an undercurrent below. For an infinite wind band the usual coastal jet regime follows. The coastal jet is trapped within the surface layer. For a finite wind band Kelvin waves exiting at the edges of the wind patch radiate alongshore with the coast to the right and arrest the surface jet and introduce the undercurrent.

The general current structure does not depend too much on the model parameters, except close to the corner point $z = -H_{\text{mix}}$ and $y = 0$, where in the inviscid case the longshore current becomes singular.

In section 5 the equatorial ocean model is forced by a steady zonal wind band. Due to the occurrence of infinite series of Hermite functions the algebra is much more complex than in the coastal ocean case, whence we have confined ourselves to the derivation of closed form expressions for the zonal current.

Apart from the assumption of constant (or weakly variable) Brunt–Väisälä frequency as well as a simple forcing and friction we have utilized the long wave approximation and some approximations of infinite series of Hermite functions associated with the Yoshida jet and the long Rossby waves.

The approximate closed solutions exhibit a reasonable current structure which consists of an arrested surface jet, the Yoshida jet, and an equatorial undercurrent. The surface current is somewhat too strong. This is due to the neglecting of meridional boundaries, as it was demonstrated by McCreary (1981a).

The gross structure of the currents depend not very much on the model parameters, except in the vicinity of the equator, where, in particular, the solution becomes singular at $z = -H_{\text{mix}}$ for a vanishing damping rate r.

For an unbounded zonal wind a pure Yoshida jet remains which is confined to the surface layer and which corresponds to the coastal jet. For a finite wind band eastward propagating Kelvin and westward propagating long Rossby waves, excited at the edges of the wind band, have arrested the surface jet and generated the equatorial undercurrent.

An important difference between the two models consist in the occurrence of the equatorial Rossby waves. Thus, particularly in the inviscid case, due to the Rossby waves the equatorial current becomes independent of the zonal coordinate x, while in the inviscid coastal ocean model the alongshore current depends linearly on the longshore coordinate, x.

For nonzero r the Rossby wave contribution to the solution is significantly smaller than those of the Yoshida and Kelvin terms. This is due to the much larger effective damping rate of the long Rossby waves, which is proportional to the meridional mode number like $4m + 3$, $m = 0, 1, 2, \cdots$.

In summary, the close relationships between the responses of the coastal and the equatorial ocean is established by the correspondence of coastal jet and Yoshida jet, as well as, by the wave processes which arrest the surface jets and introduce undercurrents.

This paper is close to the theory of McCreary (1981a,b). Its main results consist in the derivation of closed form analytical expressions of some of the dynamical variables.

Acknowledgments. The author thanks Dr. H. U. Lass for many discussions and B. Kayser for drafting the figures.

REFERENCES

Abramovitz, M., and I. A. Stegun, 1984: *Handbook of Mathematical Functions.* Verlag H. Deutsch, 268 pp.

Fennel, W., 1986: Theory of the inertial response of channel models. *Beitr. Meeresk.*, H. **54**, 3–18.

——, D. Halpern and H. U. Lass, 1987: Current spectra at the equator. *Beitr. Meeresk.*, H. **56,** 3–17.

Fjeldstad, J. E., 1963: Internal waves of tidal origin. *Geofys. Publ.*, **25,** 1–73.

Gill, A. E., 1972: Models of equatorial currents. *Proc. Symp. on Numerical Models Ocean Circulation,* Durham, Natl. Acad. Sci., 1972.

——, 1982: *Atmosphere-Ocean Dynamics,* Academic Press, 661 pp.

McCreary, J. P., 1981a: A linear stratified ocean model of the equatorial undercurrent. *Phil. Trans. Roy. Soc. London,* **A298,** 603–635.

——, 1981b: A linear stratified ocean model of the coastal undercurrent. *Phil. Trans. Roy. Soc. London,* **A302,** 385–413.

——, 1985: Modelling equatorial ocean circulation. *Annual Review of Fluid Mechanics,* Vol. 17, Annual Reviews, 359–409.

McPhaden, M. J., 1981: Continuously stratified model of the steady-state equatorial ocean. *J. Phys. Oceanogr.,* **11,** 337–354.

Moore, D. W., and S. G. H. Philander, 1977: Modelling the tropical ocean circulation. *The Sea,* Vol. 6, M. N. Hill, Ed. Interscience, 319–361.

Oberhettinger, F., 1957: *Tabellen zur Fourier Transformation.* Springer-Verlag, 214 pp.

Philander, S. G. H., and J. H. Yoon, 1982: Eastern boundary currents and coastal upwelling. *J. Phys. Oceanogr.,* **12,** 862–879.

Yoshida, K., 1959: A theory of the Cromwell current and of the equatorial upwelling—an interpretation in a similarity to a coastal circulation. *J. Oceanogr. Soc. Japan,* **15,** 159–170.